

EGRET upper limits and stacking searches of γ -ray observations of luminous and ultra-luminous infrared galaxies

Analía N. Cillis^{1,2}, Diego F. Torres³, & Olaf Reimer⁴

ABSTRACT

We present a stacking analysis of EGRET γ -ray observations at the positions of luminous and ultraluminous infrared galaxies. The latter were selected from the recently presented HCN survey, which is thought to contain the most active star forming regions of the universe. Different sorting criteria are used and, whereas no positive collective detection of γ -ray emission from these objects we determined both collective and individual upper limits. The upper most excess we find appears in the case of ULIRGs ordered by redshift, at a value of 1.8σ .

Subject headings: gamma rays: observations

1. Introduction

Luminous infrared galaxies (LIRGs) are the dominant population of extragalactic objects in the local ($z < 0.3$) universe at bolometric luminosities above $L > 10^{11} L_\odot$. Ultra luminous infrared galaxies (ULIRGs) present $L_{\text{FIR}} > 10^{12} L_\odot$, and are the most luminous local objects (see Sanders & Mirabel 1996 for a review). The most notable feature of LIRGs and ULIRGs is perhaps the large concentration of molecular gas that they have in their centers, at densities orders of magnitude larger than found in Galactic giant molecular clouds (e.g., Downes et al. 1993; Downes & Solomon 1998; Bryant & Scoville 1999). This large molecular material is believed to be the result of a merging process between two or more galaxies, in which much of the gas in the former spiral disks —particularly that located at

¹Code 661, LHEA NASA Goddard Space Flight Center, Greenbelt, MD 20771, E-mail: cillis@blazar.gsfc.nasa.gov

²Also SP Systems Inc.

³Lawrence Livermore National Laboratory, 7000 East Ave., L-413, Livermore, CA 94550, E-mail: dtorres@igpp.ucb.edu

⁴Institut für Theoretische Physik IV, Ruhr-Universität Bochum, 44780, Germany. E-mail: olr@tp4.ruhr-uni-bochum.de

distances less than 5 kpc from each of the pre-merger nuclei— has fallen together, therein triggering a huge starburst phenomenon (e.g., Sanders et al. 1988; Melnick & Mirabel 1990). LIRGs and ULIRGs thus have large CO luminosities and a high value for the ratio $L_{\text{FIR}}/L_{\text{CO}}$, both being about one order of magnitude greater than for normal spirals. The latter substantiates, based on star formation models, a greater star formation rate per unit mass of gas.

In a recent letter (Torres et al. 2004), by computing the γ -ray flux produced by the interaction between an enhanced cosmic ray population and the molecular material, ultimately leading to neutral pion decay, it was shown that LIRGs and ULIRGs are plausible sources for GLAST and the next generation of Cherenkov telescopes. This result was deepened by a detailed analysis of the γ -ray emission from Arp 220, the most extensively studied ULIRG, that included the emission of secondaries (Torres 2004). The enhanced population of relativistic particles is the result of the large number of supernovae and young stellar objects present in the central environment. The star formation rate in LIRGs is 100–1000 times larger (e.g., Gao & Solomon 2004b; Pasquali et al. 2003) and scales with the amount of dense molecular gas (traced in turn by the HCN line). It is natural to expect that the central regions of LIGs have cosmic ray enhancements comparable to the ratio between their star formation rates (SFRs) and that of the Milky Way. Torres et al. (2004) showed that if this is correct, then many of the LIRGs –particularly those located in the 100 Mpc sphere— are going to appear as individual GLAST sources.

Although detailed predictions for a particular ULIRG (Arp 220, Torres 2004) suggest that these galaxies were below EGRET sensitivity, it was yet open to discussion if they would show up in an stacking search. This search, similar to what was made by Cillis et al. (2004) for radiogalaxies, and by Reimer et al. (2003) for clusters of galaxies, is presented here. We also provide here upper limits from existing EGRET data for the fluxes of LIRGs in different energy bands, which are useful both, for future theoretical modelling and for consistency check with new sets of data.

2. Stacking technique

The general stacking method we have applied follows that outlined by Cillis et al. (2004) when studying radiogalaxies. In order to perform the stacking technique and look for a possible collective detection of the γ -ray emission from LIRGs, we have extracted rectangular sky maps with the selected target objects located at the center.

We have used EGRET data from April 1991 through September 1995 —as covered by

the Third EGRET Catalog (Hartman et al. 1999), in celestial and galactic coordinates. The extracted maps for each particular target were chosen to be $60^\circ \times 60^\circ$ in size, in order to have large off fields of views and be consistent the EGRET point spread function (PSF).

Transforming the maps to an equatorial position before co-adding them causes a substantial image distortion, except for those originally near the all-sky map equator. To minimize this distortion we have extracted maps from the all-sky map, celestial or Galactic, which had the target object closer to its equator. This was done for both, count and the exposure maps, and for all targets. We have transformed the coordinates of each map into pseudo-coordinates, with the target object at the center. After doing this, the maps were co-added, producing the stacking.

It was also necessary to extract a diffuse background map for each target object. For this purpose, we have used the diffuse model that is standard in EGRET analysis (Hunter et al. 1997). In order to take into account the existence of known EGRET sources, idealized sources with the appropriate fluxes distributed following EGRET’s PSF were added to the diffuse map. This was done only for the sources that were detected significantly during the time interval of the all-sky maps: 3EG sources that were significantly detected only during shorter sub-intervals were not considered for the background model. It was necessary to normalize each one of the extracted diffuse maps (D_i) for the different exposures (ϵ_i) of the target objects. The extracted diffuse map for each target object was also transformed into pseudo-coordinates. Finally the diffuse maps for the co-added data were obtained as: $\frac{1}{\epsilon_{tot}} \sum_i c_i$ where c_i are the counts diffuse maps ($c_i = \epsilon_i D_i$) and $\epsilon_{tot} = \sum_i \epsilon_i$.

Stacked maps for the different groups of objects analyzed below were created and results are described in the next section. To find the significance of the detection in a particular “class” we have used the EGRET likelihood ratio (Mattox et al. 1996), a formalism that produces a “test statistic” (“TS”) $TS = -2(\ln L_0 - \ln L_1)$, where L_0 and L_1 are likelihood values with and without a possible source. \sqrt{TS} is roughly equivalent to the number of standard deviations (σ).

3. Classes of LIRGS and results

We have stacked galaxies from the HCN survey (Gao & Solomon 2004a; Gao & Solomon 2004b) after sorting them using different criteria. The HCN survey is a systematic observation of 53 IR-bright galaxies, including 20 LIRGs with $L_{\text{FIR}} > 10^{11} L_\odot$, 7 with $L_{\text{FIR}} > 10^{12} L_\odot$, and more than a dozen of the nearest normal spiral galaxies. Essentially, all galaxies with strong CO and IR emission were chosen for survey observations. It also includes a litera-

ture compilation of data for another dozen IR-bright objects. This is the largest and most sensitive HCN survey of galaxies, and thus of dense interstellar mass residing there, to date.

We have excluded from our consideration those galaxies that are close to the Galactic Plane $|b| < 20^\circ$ (outer Galaxy), and $|b| < 30^\circ$ ($|l| < 50^\circ$), because the background around those objects would overwhelm any possible signal.

Table 1 shows all the galaxies in the HCN survey referred above, ordered by L_{HCN}/L_{CO} indicating their coordinates, redshift, the ratio between line luminosities $-L_{HCN}$ and $L_{CO}-$, and cosmic ray enhancement. In that Table, the column “Galactic Plane” shows whether the galaxy is within $|b| < 20^\circ$ (outer Galaxy), and $|b| < 30^\circ$ ($|l| < 50^\circ$) and thus whether that galaxy was excluded from our tests. Following Torres et al. (2004), to which we refer for details, we have computed the minimum average value of cosmic ray enhancement, dubbed k , for which the γ -ray flux above 100 MeV would be above 2.4×10^{-9} photons $\text{cm}^{-2} \text{ s}^{-1}$. The latter is approximately the GLAST satellite sensitivity after 1 yr of all-sky survey. k -values of at least a few hundreds are deemed probable, based on enhancements derived in individual supernova remnants. Luminosity distances used were those provided in the HCN survey, assuming a Hubble parameter of $H_0 = 75 \text{ km s}^{-1} \text{ Mpc}^{-1}$; although, since redshifts are very small, changes in the cosmological model do not introduce significant changes in distances. We selected the galaxies to perform the stacking technique taking into account the brightest, the nearest, those having the smaller cosmic ray enhancement needed to produce fluxes above GLAST sensitivity, and finally the ratios between the L_{HCN} and L_{CO} , and between SFR and k . In the case of the latter, those galaxies having $(SFR/SFR_{MW})/k > 1$ are believed to be particular good candidates for detection.

For each class or subclass we have generated stacked maps containing N galaxies, with $N=2, 4, 6, \text{ etc.}$ For each stacked map so generated, we have then determined the detection significance using the standard likelihood method. The results of this research are summarized in Table 2. For each sorting criterion we have specified the total number of the objects considered, the maximum detection significance, and the number of objects yielding that maximum. We have found no significant result above 1.8σ , for any class investigated and for any number of objects included. This number was obtained for the case in which all ULIRGs with $L > 10^{12}L_\odot$ were considered ordered by redshift.

In Figure 1 we show an example of the stacked maps created (maps of counts, exposure and background). The left column corresponds to the case of the highest TS obtained (the case described in the last paragraph). The middle and right column show stacked maps for LIRGs ordered by L_{HCN}/L_{CO} for 54 stacked galaxies (where the TS obtained was equal to zero), and for the first four LIRGs ordered by L_{HCN}/L_{CO} (ARP 193, MRK 273, MRK 231, UGC 05101), where the maximum TS for the class was obtained ($\sqrt{TS} = 1.2$).

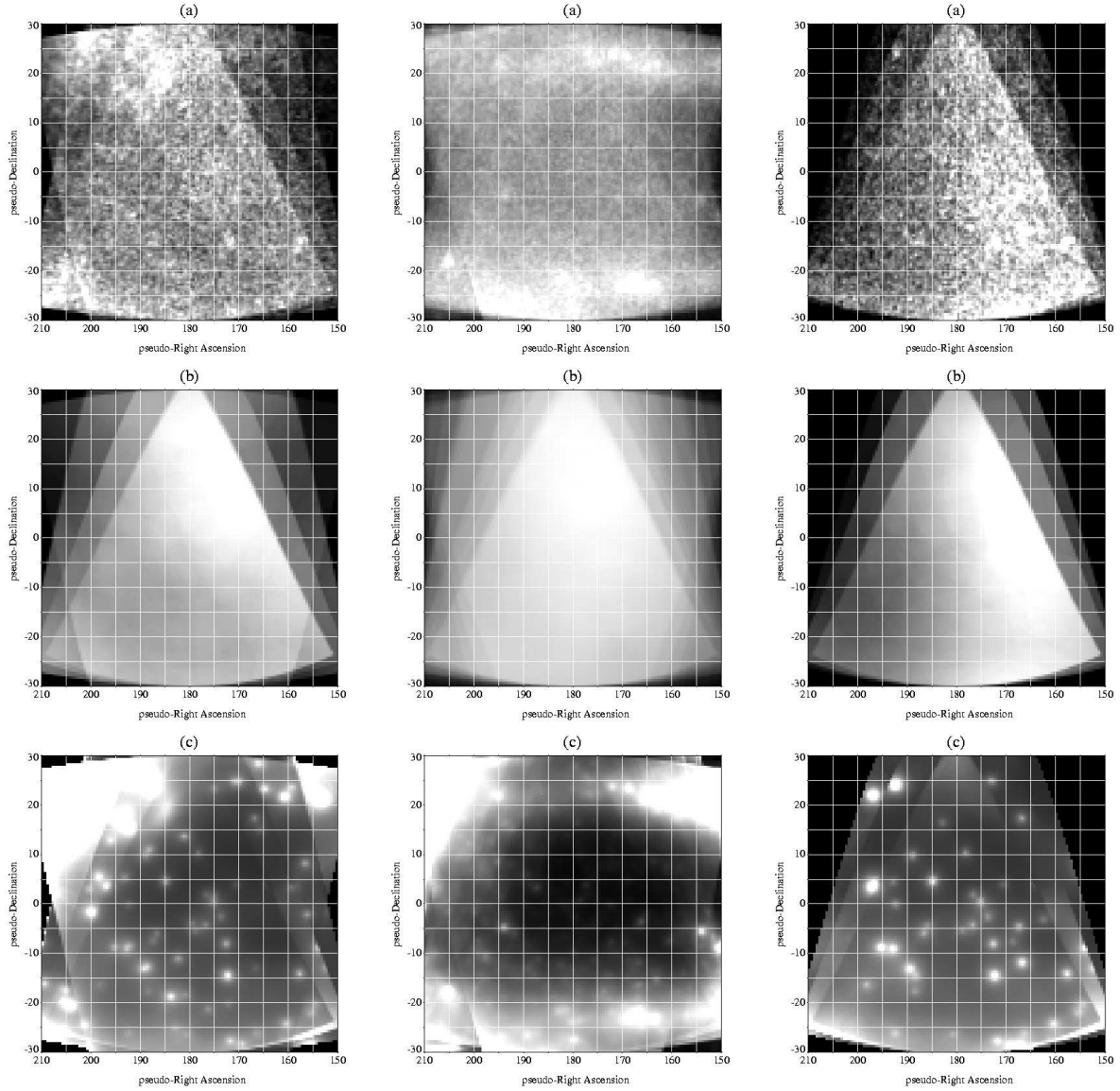


Fig. 1.— First column: Example of stacked maps for 6 ULIRGs with $L_{IR} \geq 10^{12} L_{\odot}$ ordered by redshift (ARP220, MRK 273, UGC 05101, MRK 231, 05189-2524, 10566+2448). Middle column: Example of stacked maps for 54 LIRGs ordered by L_{HCN}/L_{CO} (see Table 1). Right column: Example of stacked maps for 4 LIRGs ordered by L_{HCN}/L_{CO} (ARP193, MRK273, MRK231, UGC 05101). In all columns, (a) counts, (b) exposure (c) background. The location of interest is at pseudo-Dec 0° and pseudo-RA 180° .

Upper limits for the fluxes for all LIRGs in the HCN survey that are located away from the Galactic plane are given in Table 3, in units of 10^{-8} cm $^{-2}$ s $^{-1}$. Table 3 presents five of the sixteen energy bins where we have conducted this analysis.¹ None of the LIRGs we investigated have been individually detected, which is, in fact, consistent with the level of flux expected from LIRGs (i.e., fluxes above GLAST sensitivity but below the EGRET one (see, e.g., Torres 2004). The only galaxy for which a flux (not an upper limit) was determined is Arp 55. The flux for this galaxy, in the range 500 MeV–1 GeV was $1.9 \pm 0.6 \times 10^{-8}$ photons cm $^{-2}$ s $^{-1}$, with $TS = 26.3$. This might be thought of as suggestive for a detection, although Arp 55 was not significantly detected in consequent energy intervals, and seems not to be special otherwise. Its redshift is larger than the prototypical ULIRG, and more active galaxy, Arp 220, and moreover, its $L_{\text{HCN}}/L_{\text{CO}}$ ratio is smaller than that obtained for the former. Lastly, one expects statistical fluctuations when investigating a sample of more than 50 galaxies in 16 different energy bins.

4. Discussion

We have presented an stacking search for γ -ray emission from LIRGs and ULIRGs using data from the EGRET experiment. Our results show that these galaxies were neither individually nor collectively detected, under a variety of different sub-sampling and ranking ordering. Apart from the obvious arrangement by distance (redshifts) we have essentially explored all possible ordering parameters to investigate the preferable cases for detectability at high energy γ -rays. They included the ratio between line luminosities of HCN and CO; i.e., the ratio between the dense mass most plausible subject to higher enhancements of cosmic rays and the molecular mass less densely distributed as traced by CO. They also included the value of cosmic ray enhancement—computed under simplifying assumptions—that would make the galaxy detectable by the GLAST-LAT. Also, we considered the ordering using the ratio between the SFR in Milky Way units and the cosmic-ray enhancement, in the understanding that a realistic value for the latter should exceed the SFR. We have also imposed upper limits in different energy bands that can be used as a constraint for future multifrequency modelling. Even if we presently were not able to detect LIRGs and ULIRGs in high energy γ -rays, a suggestive excess has been found among the most active star forming regions of the sample, especially when ordered by redshift. Summarizing, LIRGs and ULIRGs, whereas not individually detected by EGRET (a result consistent with theoretical expectations) well remain a plausible candidate for GLAST and Cherenkov telescopes

¹These are 30-50, 50-70, 70-100, 100-150, 150-300, 300-500, 500-1000, 1000-2000, 2000-4000, 4000-10000, 30-100, 100-300, 300-1000, > 100 , > 300 , > 1000 MeV.

detections.

ANC would like to thank R.C. Hartman and D. L. Bertsch for useful discussions. The work of DFT was performed under the auspices of the U.S. D.O.E. (NNSA), by the University of California Lawrence Livermore National Laboratory under contract No. W-7405-Eng-48. OR acknowledges support by DLR QV0002.

Table 1. HCN Survey

NAME	1	b	G-Plane	RA	DEC	z	Mag	L_{HCN}/L_{CO}	SFR/SFR_{MW}	k	$\frac{SFR/SFR_{MW}}{k}$
*17208-0014	22.221135	19.353624	YES	260.841382	-0.283436	0.04281	15.1	0.256	1041.23077	427	2.438479555
ARP 193	82.928889	80.5998083	NO	200.1472625	34.1394972	0.02335	14.4	0.238	263.07692	452	0.582028584
*MRK 273	108.1059064	59.6818904	NO	206.1754626	55.8868475	0.03778	15.07	0.234	420.92308	746	0.564240054
MRK 231	121.6108323	60.2423486	NO	194.0593079	56.8736769	0.04217	14.41	0.226	515.07692	738	0.697936206
*UGC 05101	152.476413	42.896978	NO	143.965212	61.353137	0.03939	15.2	0.197	276.92308	1057	0.261989669
*23365+3604	106.99783	-24.268484	NO	354.755292	36.352417	0.06448	16.3	0.176	415.38462	1743	0.238315904
NGC 1068	172.1037384	-51.9337526	NO	40.6696292	-0.0132806	0.00379	9.61	0.174	99.96923	28	3.570329643
*10566+2448	212.455124	64.688165	NO	164.825577	24.542855	0.0431	15.7	0.166	282.46154	1022	0.276381155
NGC 6921	66.983282	-7.558412	YES	307.12025	25.723417	0.01429	14.4	0.16	77.81538	435	0.178885931
NGC 6240	20.728994	27.291006	YES	253.245375	2.400944	0.02448	13.8	0.139	304.61538	255	1.194570118
IC 5179	6.502243	-55.927177	NO	334.037917	-36.843722	0.01141	12.38	0.129	94.70769	169	0.560400533
*ARP 220	36.627128	53.02893	NO	233.737985	23.503187	0.01813	13.94	0.117	254.76923	149	1.709860604
*05189-2524	227.779961	-30.749102	NO	79.743025	-25.412818			0.093	171.69231	906	0.189505861
NGC 5135	311.747863	32.45034	NO	201.433583	-29.833667	0.01372	12.88	0.087	75.6	179	0.422346369
ARP 148	174.18998	63.98563	NO	165.97167	40.84917	0.03452		0.085	110.76923	914	0.121191718
*VIIIZw31	133.180207	22.614913	NO	79.1935	79.670167	0.05367	15.8	0.078	271.38462	835	0.325011521
ARP 299	141.898935	55.407582	NO	172.139559	58.563144	0.01041	11.98	0.072	58.15385	133	0.437246992
NGC 2146	135.653411	24.896351	NO	94.657125	78.357028	0.00298	11.38	0.071	26.58462	39	0.681656923
NGC 7130	9.943251	-50.352306	NO	327.08125	-34.951306	0.01615	12.98	0.071	90.55385	197	0.459664213
NGC 7771	104.26359	-40.573953	NO	357.853667	20.111833	0.01427	13.08	0.07	180	84	2.142857143
IC 1623	145.196075	-79.665042	NO	16.946583	-17.507028	0.02007		0.065	235.38462	107	2.199856262
MRK 331	104.461088	-40.124167	NO	357.861677	20.586075	0.01848	14.87	0.064	92.76923	228	0.406882588
NGC 253	97.369238	-87.964044	NO	11.888002	-25.28822	0.0008	8.04	0.059	7.47692	3	2.492306667
NGC 7469	83.0985253	-45.4666436	YES	345.8150955	8.8739973	0.01632	13	0.059	60.64615	257	0.235977237
NGC 3893	148.155029	65.227411	NO	177.159125	48.710833	0.00323	11.16	0.056	6.36923	99	0.064335657
NGC 1365	237.956197	-54.598032	NO	53.401548	-36.140402	0.00546	10.32	0.053	85.84615	15	5.723076667
M82	141.409718	40.566798	NO	148.96758	69.679704	0.00068	9.3	0.053	8.30769	4	2.0769225
NGC 6946	95.718973	11.672974	YES	308.718068	60.153946	0.00016	9.61	0.053	13.56923	7	1.938461429
NGC 5775	359.431609	52.423009	NO	223.489988	3.544458	0.00561	12.24	0.052	15.78462	87	0.181432414
NGC 1614	204.451101	-34.381535	NO	68.499394	-8.578883	0.01594	13.63	0.051	34.61538	341	0.101511378
IC 342	138.172575	10.579954	YES	56.702125	68.096111	0.0001	9.1	0.05	13.01538	3	4.33846
NGC 5005	101.6143082	79.2490978	NO	197.7342958	37.0592056	0.00316	10.61	0.049	11.35385	50	0.227077
NGC 1022	179.0179945	-57.3715587	NO	39.6362718	-6.6774286	0.00485	12.09	0.047	5.53846	222	0.024948018
NGC 4945	305.272076	13.3398849	YES	196.3644897	-49.4682129	0.00187	9.3	0.047	7.47692	5	1.495384
18293-3413	0.1481729	-11.3073324	YES	278.171375	-34.1909722	0.01818		0.047	111.6	127	0.878740157

Table 1—Continued

NAME	l	b	G-Plane	RA	DEC	z	Mag	L_{HCN}/L_{CO}	SFR/SFR_{MW}	k	$\frac{SFR}{SFR_{MW}}$
NGC 695	140.583698	-38.230978	NO	27.809342	22.582363	0.03247	13.84	0.046	119.07692	401	0.296949925
NGC 4041	132.701938	54.047245	NO	180.55075	62.137278	0.00412	11.88	0.046	4.98462	174	0.028647241
MRK 1027	157.758852	-52.01998	NO	33.52329	5.173238	0.03022		0.045	52.33846	765	0.068416288
NGC 5678	100.044725	54.504871	NO	218.023208	57.921444	0.00641	12.13	0.044	20.76923	94	0.220949255
M 83	314.583573	31.972746	NO	204.253833	-29.86575	0.00172	8.2	0.043	9.69231	4	2.4230775
NGC 3079	157.810244	48.359895	NO	150.490827	55.679743	0.00375	11.54	0.042	27.69231	23	1.204013478
NGC 7479	86.270769	-42.841757	NO	346.236042	12.322889	0.00794	11.6	0.042	31.01538	97	0.319746186
NGC 6701	90.396653	24.401574	NO	280.801917	60.653333	0.01323	13.01	0.041	38.21538	199	0.192037085
NGC 7331	93.7219374	-20.7241007	NO	339.2670653	34.4156372	0.00272	10.35	0.041	12.18462	44	0.276923182
NGC 520	138.705785	-58.060572	NO	21.146125	3.792417	0.00761		0.039	17.72308	124	0.142928065
NGC 2276	127.669983	27.709215	NO	111.809833	85.754556	0.00804	11.93	0.039	11.07692	258	0.042933798
NGC 4631	142.805542	84.223494	NO	190.533375	32.5415	0.00202	9.75	0.037	2.21538	60	0.036923
NGC 660	141.60674	-47.346341	NO	25.759792	13.645667	0.00283	12.02	0.036	7.2	56	0.128571429
NGC 2903	208.711567	44.540153	NO	143.042125	21.500833	0.00186	9.68	0.036	2.49231	35	0.071208857
NGC 4030	277.370075	59.214755	NO	180.0985	-1.1	0.00487	12.01	0.036	14.95385	40	0.37384625
NGC 3628	240.851695	64.780866	NO	170.070917	13.5895	0.00281	10.28	0.034	6.64615	17	0.39095
NGC 4414	174.538951	83.181944	NO	186.612917	31.223528	0.00239	10.96	0.033	4.43077	39	0.113609487
ARP 55	176.29697	43.9411	NO	138.97958	44.33194	0.0393		0.03	105.23077	443	0.237541242
NGC 4826	315.680884	84.421337	NO	194.182333	21.681083	0.00136	9.36	0.03	1.10769	36	0.030769167
NGC 1055	171.331191	-51.749461	NO	40.438458	0.443167	0.00332	11.4	0.028	10.24615	34	0.301357353
NGC 5713	351.023352	52.123848	NO	220.048042	-0.289222	0.00658	12.18	0.027	6.09231	149	0.040887987
M 51	104.8513511	68.5608401	NO	202.4696292	47.1951722	0.00154	8.96	0.026	13.84615	10	1.384615
NGC 1144	175.8754354	-49.8886843	NO	43.8008169	-0.1835573	0.02885	13.78	0.025	73.93846	264	0.280069924
NGC 891	140.383473	-17.413846	YES	35.639224	42.349146	0.00176	10.81	0.024	6.92308	20	0.346154
NGC 828	139.188076	-21.183497	NO	32.539875	39.190361	0.01793	13.15	0.022	36	203	0.177339901
NGC 1530	135.22306	17.764624	YES	65.862917	75.295583	0.00821	12.25	0.021	13.56923	114	0.119028333
NGC 3556	148.314482	56.251842	NO	167.879042	55.674111	0.00233	10.69	0.02	2.49231	52	0.047929038
NGC 3627	241.96111	64.418688	NO	170.062615	12.991549	0.00243	9.65	0.017	2.21538	27	0.082051111
NGC 3147	136.2899917	39.463239	NO	154.2235454	73.4007486	0.00941	11.43	0.015	24.92308	55	0.453146909
NGC 5055	105.996973	74.28768	NO	198.955542	42.029278	0.00168	9.31	0.012	2.76923	13	0.213017692

Note. — The table shows some properties of the galaxies in the HCN Survey. LIGs with $L_{IR} \geq 10^{11} L_{\odot}$ are highlighter in boldface and ULIGs with $L_{IR} \geq 10^{12} L_{\odot}$ are further indicated by *. The column “G-Plane” indicates if the galaxy is near the Galactic Plane. In that case the galaxy (case “YES”) was excluded from consideration in our analysis.

Table 2. The HCN survey results

Subclass	Sorting Criteria	Max N. ^a	Max \sqrt{TS} ^b	N. Y Max ^c
ALL	Distance (Mpc)	36	0.7	18
ALL	$(SFR/SFR_{MW})/k$	54	0.4	6
ALL	L_{HCN}/L_{CO}	54	1.2	4
ALL	k-factor	26	1.1	20
ULiGs $L > 10^{12}L_{sol}$	red shift	8	1.8	6
ULiGs $L > 10^{12}L_{sol}$	$(SFR/SFR_{MW})/k$	8	1.3	2
ULiGs $L > 10^{12}L_{sol}$	L_{HCN}/L_{CO}	8	0.5	4
$L > 10^{11}L_{sol}$	$(SFR/SFR_{MW})/k$	24	0.7	6
$L > 10^{11}L_{sol}$	L_{HCN}/L_{CO}	24	1.2	4

^aMaximum number of objects considered.

^bMaximum \sqrt{TS} found.

^cNumber of objects yielding the maximum \sqrt{TS} .

Table 3. Flux Upper Limits

Name	Energy range [MeV]				
	100-300	300-1000	>100	>300	>1000
ARP 193	5	1	4	1	1
MRK 273	4	1	3	1	0
MRK 231	6	1	6	2	1
UGC 05101	7	1	5	1	0
23365+3604	6	2	5	2	1
NGC 1068	4	1	4	1	1
10566+2448	4	1	3	1	0
IC 5179	6	1	5	2	1
ARP 220	6	3	6	3	1
05189-2524	8	2	9	3	2
NGC 5135	4	2	3	2	0
ARP 148	3	1	3	1	0
VIZW31	4	1	3	1	1
ARP 299	3	1	2	1	0
NGC 2146	3	1	3	1	0
NGC 7130	5	2	5	3	2
NGC 7771	9	3	8	4	2
IC 1623	5	2	4	2	1
MRK 331	10	2	8	4	2
NGC 253	6	1	8	2	2
NGC 3893	3	1	3	1	0
NGC 1365	5	1	5	2	1
M82	3	1	3	1	0
NGC 5775	9	2	5	2	1
NGC 1614	6	2	5	1	1
NGC 5005	5	1	4	1	1
NGC 1022	4	1	4	2	1
NGC 695	5	1	4	1	1
NGC 4041	3	1	2	1	1
MRK 1027	5	1	4	1	1
NGC 5678	4	1	3	1	1
M83	4	1	3	1	0
NGC 3079	3	1	3	2	1
NGC 7479	5	2	4	2	0
NGC 6701	10	6	12	6	1
NGC 7331	7	2	8	2	1
NGC 2276	4	3	5	4	1
NGC 520	7	2	7	2	1
NGC 4631	3	1	3	1	0
NGC 660	5	1	6	1	1
NGC 2903	4	1	4	1	1
NGC 4030	3	1	2	1	1
NGC 3628	3	2	5	2	0
NGC 4414	5	2	3	2	1

Table 3—Continued

Name	Energy range [MeV]				
	100-300	300-1000	>100	>300	>1000
ARP 55	4	2	4	2	2
NGC 4826	4	1	4	1	0
NGC 1055	4	1	4	1	1
NGC 5713	5	1	4	1	0
M51	8	3	7	3	1
NGC 1144	4	1	4	2	2
NGC 828	9	1	8	2	1
NGC 3556	3	1	2	1	0
NGC 3627	3	2	5	2	0
NGC 3147	4	1	4	1	0
NGC 5055	6	1	6	1	1

Note. — Energy values are in MeV and fluxes in units of 10^{-8} photons cm^{-2} s^{-1} .

REFERENCES

Cillis A. N., Hartman R. C. & Bertsch D. L. 2004, *ApJ* 601, 142

Bryant P. M., & Scoville N. Z. 1999, *ApJ* 117, 2632

Downes, D., Solomon, P. M., & Radford, S. J. E. 1993, *ApJ*, 414, L13

Downes, D., & Solomon, P.M. 1998, *ApJ*, 507, 615

Hartman R. C. et al. 1999, *ApJS* 123, 79

Hunter S. D. et al. 1997, *ApJ* 481, 205

Mattox J. R. et al. 1996, *ApJ* 461, 396

Melnick J. & Mirabel I. F. 1990, *A&A* 231, L19

Gao Y. & Solomon P. M. 2004a, *ApJ Suppl.* 152, 63

Gao Y. & Solomon P. M. 2004b, *ApJ* 606, 271

Pasquali A., Gallagher J. S., & de Grijs, R. 2003, *A&A* 415, 103

Reimer O., Pohl M., Sreekumar P. & Mattox J. R. 2003, *ApJ* 588, 155

Sanders D. B. et al. 1988, *ApJ* 325, 74

Sanders D. B., & Mirabel I. F. 1996, *ARA&A*, 34, 749

Torres D. F., Romero G. E., Dame T. M., Combi J. A. & Butt Y. M. 2003, *Physics Reports* 382, 303

Torres D. F. 2004, arXiv:astro-ph/0407240. To appear in *ApJ*.

Torres D. F., Reimer O., Domingo-Santamaría E. & Digel S. 2004, *ApJ* 607, L99